

# scFlow: A Scalable and Reproducible Analysis Pipeline for Single-Cell RNA Sequencing Data

Combiz Khozoie<sup>1,2</sup>, Nurun Fancy<sup>1,2</sup>, Mahdi M. Marjaneh<sup>1,2</sup>, Alan E. Murphy<sup>1,2</sup>, Paul M. Matthews<sup>1,2</sup>, and Nathan Skene<sup>1,2</sup>

<sup>1</sup>UK Dementia Research Institute, Imperial College London

<sup>2</sup>Department of Brain Sciences, Imperial College London, United Kingdom

August 19, 2021

## <sup>1</sup> Abstract

<sup>2</sup> Advances in single-cell RNA-sequencing technology over the last decade have enabled exponential increases in throughput: datasets with over a million cells are becoming commonplace. The burgeoning scale of data generation, combined with the proliferation of alternative analysis methods, led us to develop the scFlow toolkit and the nf-core/scflow pipeline for reproducible, efficient, and scalable analyses of single-cell and single-nuclei RNA-sequencing data. The scFlow toolkit provides a higher level of abstraction on top of popular single-cell packages within an R ecosystem, while the nf-core/scflow Nextflow pipeline is built within the nf-core framework to enable compute infrastructure-independent deployment across all institutions and research facilities. Here we present our flexible pipeline, which leverages the advantages of containerization and the potential of Cloud computing for easy orchestration and scaling of the analysis of large case/control datasets by even non-expert users. We demonstrate the functionality of the analysis pipeline from sparse-matrix quality control through to insight discovery with examples of analysis of four recently published public datasets and describe the extensibility of scFlow as a modular, open-source tool for single-cell and single nuclei bioinformatic analyses.

## <sup>14</sup> Introduction

<sup>15</sup> Single-cell RNA sequencing (scRNA-seq) has enabled transcriptomic profiling at single-cell resolution, providing unprecedented insight into gene expression within cell populations ([Shema et al., 2019](#)). However, a satisfactory framework for standardized, computationally efficient analyses of scRNA-seq (or snRNA-seq) data has not been available to date. Lack of full

19 community agreement on quality measures and standards for quality control, typically large  
20 analytical batch effects and multiple parameter optimisations necessary in current tools have  
21 confounded reproducibility of results. Moreover, the burgeoning scale of scRNA-seq datasets  
22 made possible by technological advances including integrated fluidic circuits, nanodroplets,  
23 and *in situ* barcoding, has led to a concomitant increase in computational demands for in-  
24 dividual dataset, underscoring a need for efficient scaling, particularly with recognition of the  
25 value of meta-analyses (Aldridge and Teichmann, 2020). A comprehensive solution to these  
26 challenges has not been provided (Eisenstein, 2020). Nonetheless, the benefits of reproducible  
27 computational practices in the life sciences are clear and a source of extensive discourse in the  
28 literature (Baker, 2016; Perkel, 2020). The demand from governments, funders, and publishers  
29 for FAIR (findable, accessible, interoperable, and reusable) standards in data-driven sciences is  
30 highly pertinent to scRNA-seq analyses (Sansone et al., 2019). Better realisation of these goals  
31 for scRNA-seq can be promoted by standardisation of core elements in analysis pipelines to  
32 enable common approaches to annotating data for quality and its characterisation. Common  
33 metrics and a scalable analytical framework would better enable the integration, re-use, and re-  
34 purposing of published datasets within and across diseases to drive novel discoveries (Grüning  
35 et al., 2018). Challenges toward the development of such a pipeline include the deluge of compu-  
36 tational techniques for key analytical steps (Heiser and Lau, 2020), interoperability challenges  
37 between analytical tools (Tekman et al., 2020), the extensiveness of complete parameter speci-  
38 fications (Raimundo et al., 2020), the iterative nature of hyperparameter optimisation (Menon,  
39 2019), the complexity of software dependencies for end-to-end analyses (Gruening et al., 2018),  
40 and the need for flexibility to handle complex experimental designs (Luecken and Theis, 2019).

41 To this end, we have developed scFlow, an open-source analysis pipeline comprising i) the scFlow  
42 toolkit built in R with high levels of abstraction on top of popular single-cell analysis tools (e.g.  
43 Seurat, Monocle, Scater) and ii) nf-core/scFlow, a version-controlled, citable, NextFlow pipeline  
44 for the efficient orchestration of reproducible scRNA-seq analyses with scFlow (Di et al., 2017).  
45 Comprehensive reports with publication-quality figures detailing QC metrics, clustering, differ-  
46 ential expression and pathway analyses are automatically generated. The modular nature of the  
47 scFlow toolkit provides the flexibility to specify alternate algorithms for key analytical steps  
48 while capturing analysis parameters comprehensively and generating interactive reports and

49 publication-quality outputs. The nf-core/scFlow NextFlow workflow, which is engineered to  
50 follow strict best-practices guidelines of the nf-core community framework, enables “one-click”  
51 scRNA-seq analyses for users that apply easily specifiable analytical parameters and experimen-  
52 tal design specifications to orchestrate reproducible and portable (computational infrastructure-  
53 independent) analyses inside containerized environments (Ewels et al., 2020). The extensibility  
54 and modular design of scFlow should enable future updates to incorporate new methods in the  
55 field. Below, we briefly summarize the core features of scFlow and its application to published  
56 single-cell datasets.

57

## 58 **Implementation**

### 59 **Overview**

60 scFlow is comprised of two components: i) an independent R package, scFlow, containing a  
61 toolkit for analysis of single-cell RNA sequencing data and ii) a Nextflow pipeline, nf-core/scflow,  
62 for orchestrating end-to-end, reproducible, automated and scalable single-cell analyses using the  
63 scFlow R package (Fig. 1).

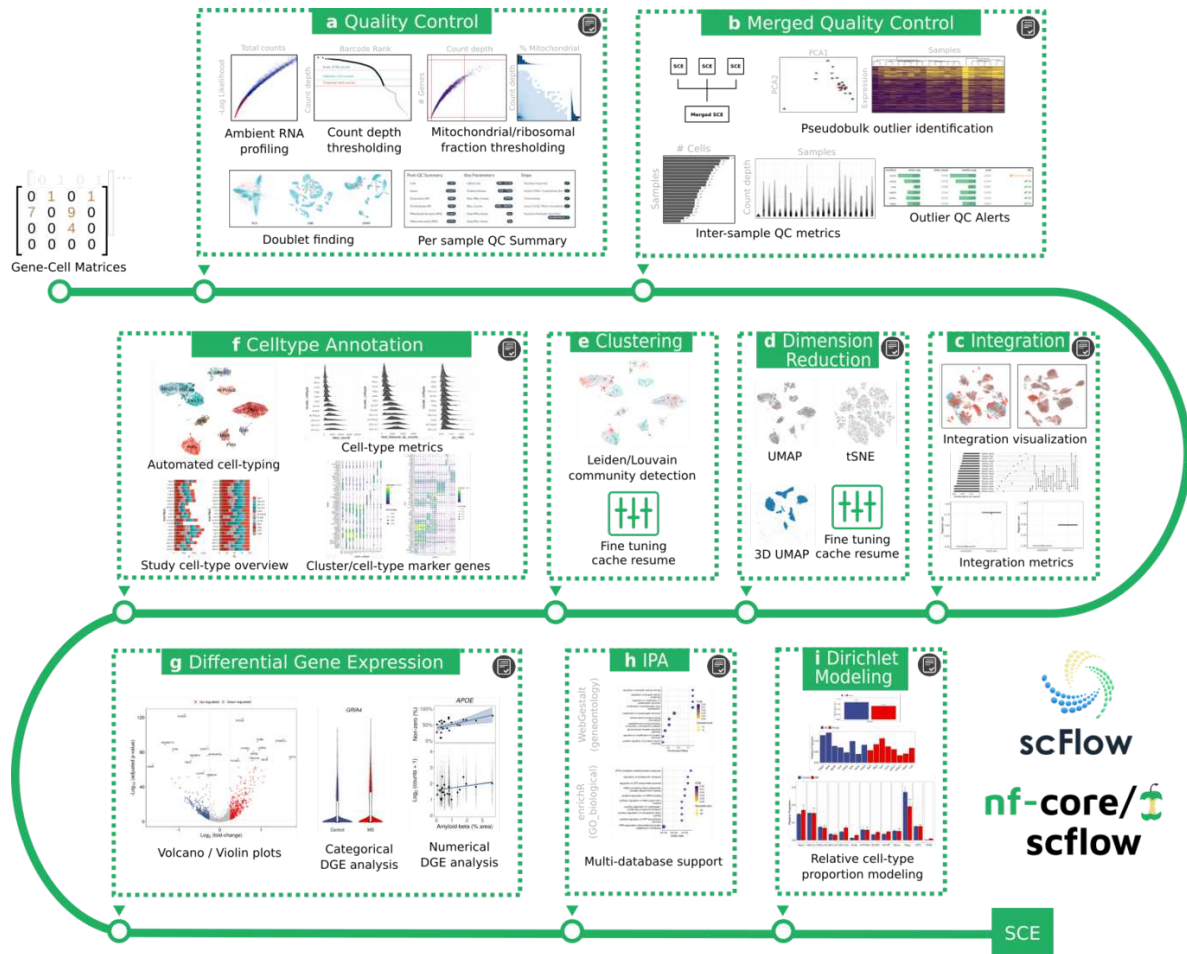


Figure 1: **Single-cell analysis pipeline with nf-core/scflow using the scFlow toolkit.** Gene-cell matrices from multi-sample case/control studies are analysed reproducibly across major analytical steps: (a) individual sample quality control including ambient RNA profiling, thresholding, and doublet/multiplet identification, (b) merged quality control including inter-sample quality metrics and sample outlier identification, (c) dataset integration with visualization and quantitative metrics of integration performance, (d) flexible dimension reduction with UMAP and/or tSNE, (e) clustering using Leiden/Louvain community detection, (f) automated cell-type annotation with rich cell-type metrics and marker gene characterization, (g) flexible differential gene expression for categorical and numerical dependent variables, (h) impacted pathway analysis with multiple methods and databases, and (i) Dirichlet modeling of cell-type composition changes. A high-quality, fully annotated, quality-controlled SingleCellExperiment (SCE) object is output for additional downstream tertiary analyses. Interactive HTML reports are generated for each analytical step indicated (grey icon). Analyses are efficiently parallelized where relevant (steps a,g,h, and i) and all steps benefit from NextFlow cache enabling parameter tuning with pipeline resumption, particularly useful for dimension reduction (d) and clustering (e).

64 The scFlow R package is built to enable standardized workflows following best practices on top of  
65 popular single-cell R packages, including Seurat, Monocle, scater, emptyDrops, DoubletFinder,  
66 LIGER, and MAST (Hao et al., 2021; Cao et al., 2019; McCarthy et al., 2017; Lun et al., 2019;  
67 McGinnis et al., 2019; Welch et al., 2019). scFlow provides the ability to undertake common an-  
68 alytical tasks required by users that involve multiple tools with a single command (i.e. a higher  
69 level of abstraction). The Bioconductor SingleCellExperiment class (Amezquita et al., 2020)  
70 is utilized throughout, with the interconversion between package-specific object classes handled  
71 “under-the-hood” to perform analytical steps and return their results seamlessly. Analytical  
72 parameters are recorded comprehensively and made readily available to enable reproducible op-  
73 timizations of analyses. Interactive HTML reports are generated for each stage of the analysis  
74 that describes algorithm performance metrics and provide publication-quality plots of a wide  
75 range of outputs, along with bibliographic citations for the analytical packages used. These re-  
76 ports thus provide the user with informative summaries of their specific analytical steps in ways  
77 that can highlight the impact of parameter choices and guide their revision when needed. The  
78 use of modular functions which receive and return a SingleCellExperiment object with relevant  
79 metadata appended allows new algorithms to be readily implemented. The following example  
80 illustrates a complete sample quality-control with default parameters using scFlow in R, includ-  
81 ing ambient RNA profiling, gene/cell annotation, thresholding, doublet/multiplet removal, and  
82 generation of an interactive HTML report with key plots: -

```
83 sce <- read_sparse_matrix(matrix_path) %>%  
84 generate_sce(metadata) %>%  
85 find_cells() %>%  
86 annotate_sce() %>%  
87 filter_sce() %>%  
88 find_singlets() %>%  
89 filter_sce() %>%  
90 report_qc_sce()
```

91 **Analytical steps with scFlow**

92 **Quality-control**

93 Initial quality-control is performed individually for each sample (Fig. 1a), using the post-  
94 demultiplexed sparse gene-cell counts matrix as input. Each sparse matrix is combined with  
95 unique sample metadata to generate the initial SingleCellExperiment (SCE) object. Ambient  
96 RNA profiling is performed optionally, using the EmptyDrops algorithm to flag and subse-  
97 quently filter cellular barcodes which do not deviate from an ambient RNA expression profile  
98 representing cell-free transcripts (Lun et al., 2019). The SCE is subsequently annotated with  
99 rich gene and cell-level metrics and appended with key plots to guide parameter selection ac-  
100 cording to best practices, including barcode rank plots, and histograms of total counts, total  
101 features, and relative mitochondrial and ribosomal gene counts (Luecken and Theis, 2019).  
102 The ability to adaptively threshold cell metrics based on median absolute deviations enables  
103 consistent thresholding criteria to be applied across samples with different characteristics (e.g.  
104 between batches, across data from different species) to support integrative analyses.

105 The pipeline provides an option for submitting filtered post-QC SCE for doublet/multiplet  
106 detection using the DoubletFinder algorithm (McGinnis et al., 2019). Cells are embedded in  
107 reduced dimensional space using PCA, tSNE, and UMAP to facilitate visualization of putative  
108 non-singlets (which typically form isolated clusters or are embedded at the peripheries of major  
109 clusters) identified by the algorithm. A post-QC summary report brings relevant plots and  
110 algorithm performance metrics together to facilitate the joint consideration of QC covariates  
111 in univariate thresholding decisions, consistent with best practices (Luecken and Theis, 2019)  
112 (File 1).

113 **Hosted file**

114 File\_1\_Zhou\_et\_al\_human\_dimis\_qc\_report.html available at <https://authorea.com/users/226952/articles/480342-scflow-a-scalable-and-reproducible-analysis-pipeline-for-single-cell-rna-sequencing-data>

117 Following the merging of multiple post-QC samples, an additional post-merge QC step is applied  
118 to evaluate comparative metrics of sample quality (Fig. 1b). Firstly, a “bulk” RNA seq PCA

119 plot of samples is generated by pseudobulking counts by sample, with an additional hierarchical  
120 clustering plot of binarized gene expressivity to highlight samples with a divergent feature space.  
121 Next, the total number of cells contributed by each sample is determined, and violin plots and  
122 interactive tables are generated for each user-specified cellular variable of interest (e.g. total  
123 counts, total features, relative mitochondrial counts, etc.), optionally stratified by experimental  
124 variables (e.g. batch). The tables additionally provide outlier warnings ( $[?2\sigma]$ ) and alerts ( $[?3\sigma]$ )  
125 for each sample QC metric. Together, these results are collated in a post-merge QC report (File  
126 2) both to guide the identification of putative sample-level outliers and any required revisions  
127 of QC parameters.

## 128 **Hosted file**

129 `File_2_Mathys_et_al_merged_report.html` available at <https://authorea.com/users/226952/articles/480342-scflow-a-scalable-and-reproducible-analysis-pipeline-for-single-cell-rna-sequencing-data>

## 132 **Integration and dimensionality reduction**

133 Latent metagene factors representing shared features of cell identity across different experimen-  
134 tal samples can be generated using the linked inference of genomic experimental relationships  
135 (LIGER) algorithm (Fig. 1c) (Welch et al., 2019). Providing these latent factors as inputs  
136 in place of principal components for dimensionality reduction can improve dataset integra-  
137 tion. Dimensionality reduction then is performed using the uniform manifold approximation  
138 and projection (UMAP) or t-distributed stochastic neighbour embedding (tSNE) algorithms to  
139 generate 2D or 3D embeddings (Fig. 1) (Kobak and Berens, 2019; Becht et al., 2018). The  
140 performance of any dataset integrations can subsequently be assessed across user-specified ex-  
141 perimental covariates (e.g. batch, sex, disease) using a combination of juxtaposed reduced  
142 dimension plots with and without integration and quantitative scores of cell mixing using ‘re-  
143 jection rates’ from the k-nearest-neighbor batch-effect (kBET) algorithm (üttner2019?). These  
144 results, together with details of the latent factors generated by LIGER (e.g. UpSet plots of  
145 dataset participation), are brought together in an integration report that serves to characterise  
146 performance of the integration algorithm and thus can be used to guide revisions of integration  
147 and dimensionality reduction parameters (Fig. 1c) (File 3).

148 **Hosted file**

149 `File_3_Ximerakis_et_al_integrate_report.html` available at <https://authorea.com/users/226952/articles/480342-scflow-a-scalable-and-reproducible-analysis-pipeline-for-single-cell-rna-sequencing-data>

152 **Clustering and cell-type annotation**

153 Cell clusters are identified with the Leiden or Louvain community detection algorithms imple-  
154 mented in Monocle using the UMAP or tSNE embeddings as inputs (Fig. 1e) (Traag et al., 2019;  
155 Trapnell et al., 2014). Following clustering, automated cell-type prediction is performed on cell  
156 clusters using the expression weighted cell type enrichment (EWCE) algorithm against reference  
157 datasets previously generated with EWCE (Fig. 1f) (Skene and Grant, 2016). Detailed cell-type  
158 metrics are subsequently generated, including plots of the relative proportions of cell-types by  
159 user-specified experimental variables (e.g. sample, diagnosis), histograms of user-specified cell  
160 metrics (e.g. total counts, total features, relative mitochondrial counts) and detailed dot-plots  
161 and interactive tables of cluster and cell-type marker genes generated using Monocle (Trapnell  
162 et al., 2014). These results are collated into a comprehensive cell-type metrics report (File 4),  
163 enabling multi-parametric characterisation of cell types and guiding any subsequent manual  
164 revisions of cell-type labels or clustering parameters that may be demanded.

165 **Hosted file**

166 `File_4_Mathys_et_al_celltype_metrics_report.html` available at <https://authorea.com/users/226952/articles/480342-scflow-a-scalable-and-reproducible-analysis-pipeline-for-single-cell-rna-sequencing-data>

169 **Differential gene expression and impacted pathway analysis**

170 Differential gene expression (DGE) within cell-types can be evaluated for both categorical (e.g.  
171 diagnosis) and numerical (e.g. age, pathology scores) dependent variables while accommodating  
172 complex experimental designs and controlling for covariates (Fig. 1g). A pre-processing step  
173 enables optional filtering of genes based on expressivity, pseudobulking, input matrix transfor-  
174 mation (e.g. Log2, CPM), and co-variate scaling and centering. The default DGE method  
175 in scFlow is a generalized linear mixed model (GLMM) with a random effect (RE) term (e.g.,

176 to account for correlations within individual samples) as implemented within the model-based  
177 analysis of single-cell transcriptomics (MAST) algorithm (Zimmerman et al., 2021; Finak et al.,  
178 2015). An interactive DGE HTML report with a volcano plot and searchable tables is genera-  
179 ted, including details of model parameters, inputs, and outputs (File 5).

180 **Hosted file**

181 `File_5_Mathys_et_al_Oligo_MASTZLM_Control_vs_pathological_diagnosisAD_de_report.html`  
182 available at <https://authorea.com/users/226952/articles/480342-scflow-a-scalable->  
183 [and-reproducible-analysis-pipeline-for-single-cell-rna-sequencing-data](https://authorea.com/users/226952/articles/480342-scflow-a-scalable-and-reproducible-analysis-pipeline-for-single-cell-rna-sequencing-data)

184 Impacted pathway analysis (IPA) is performed on DGE tables to identify enrichment of diffe-  
185 rentially expressed genes in specific pathways (Fig. 1h). Comprehensive methods and databases  
186 available within the enrichR (Kuleshov et al., 2016), ROntoTools (Khatri et al., 2007), and  
187 WebGestaltR (Liao et al., 2019) packages can be used simultaneously for the generation of  
188 an interactive HTML report including dot-plots for the top enriched pathways and searchable  
189 tables of results across different methods (File 6).

190 **Hosted file**

191 `File_6_Mathys_et_al_Oligo_MASTZLM_Control_vs_pathological_diagnosisAD_DE_ipa_report.html`  
192 available at <https://authorea.com/users/226952/articles/480342-scflow-a-scalable->  
193 [and-reproducible-analysis-pipeline-for-single-cell-rna-sequencing-data](https://authorea.com/users/226952/articles/480342-scflow-a-scalable-and-reproducible-analysis-pipeline-for-single-cell-rna-sequencing-data)

194 **Modeling of relative cell-type proportions**

195 Statistically significant changes in cell-type composition across categorical dependent variables  
196 (e.g. case vs control) can be examined using a Dirichlet-multinomial regression model, which  
197 accounts for dependencies in cell-type proportions within samples (Fig. 1i) (Smillie et al., 2019).  
198 Adjusted p-values and plots of relative abundance are generated for each cell-type and collated  
199 in an HTML report together with composition matrices used in model generation (File 7).

200 **Hosted file**

201 `File_7_Ximerakis_et_al_dirichlet_report.html` available at <https://authorea.com/>  
202 [users/226952/articles/480342-scflow-a-scalable-and-reproducible-analysis-](https://authorea.com/users/226952/articles/480342-scflow-a-scalable-and-reproducible-analysis-)

203 `pipeline-for-single-cell-rna-sequencing-data`

204 **Pipeline orchestration with nf-core/scflow**

205 **Overview**

206 We built the nf-core/scflow pipeline using Nextflow within the nf-core framework to enable  
207 standardized, portable, and reproducible analyses of case/control single-cell RNA sequencing  
208 data (Ewels et al., 2020). Pipelines built using Nextflow inherit its portability, native support  
209 for container technologies, and features including cache-based pipeline resume capability and  
210 amenability to live-monitoring (Di et al., 2017). The nf-core framework provides a means  
211 to produce high-quality, best-practices analysis pipelines with Nextflow which are ready for  
212 deployment across all institutions and research facilities (Ewels et al., 2020).

213 **Workflow**

214 The codebase for both the scFlow R package toolkit and the nf-core/scflow pipeline are stored  
215 in open-source GitHub repositories (Fig. 2). Both repositories are version controlled and uti-  
216 lize continuous integration (CI) workflows to ensure code updates pass build and functionality  
217 tests. In addition, updates to nf-core/scflow trigger an automated CI action to validate that  
218 the analysis of a small case/control dataset runs to completion without errors. Version updates  
219 to the scFlow R package trigger a CI action to build a new version-tagged Docker image which  
220 is uploaded to a Docker registry. This image is built from a Dockerfile specification which addi-  
221 tionally installs the complete set of software dependencies, including 414 versioned R packages  
222 and additional system-level dependencies (scFlow 0.7.1, see supplemental data).

223 The execution of an nf-core/scFlow pipeline run automatically retrieves the correct version of  
224 the Docker image from the Docker registry and generates reproducible containerized analysis  
225 environments for each analytical process using Docker or Singularity. Analyses are performed on  
226 the compute platform preferred by the user given the potential for implementation on local, high-  
227 performance computing cluster (HPC) or in Cloud based environments (Di et al., 2017) (Fig.  
228 2). Live-monitoring of pipeline progress is possible using Nextflow Tower [<https://tower.nf/>],  
229 a hosted and open-source solution providing live statistics on resource usage (e.g. CPU, RAM,  
230 IO, time) and cost (for Cloud analyses). Pipeline runs can also be optionally launched directly

231 from within the Nextflow Tower GUI.

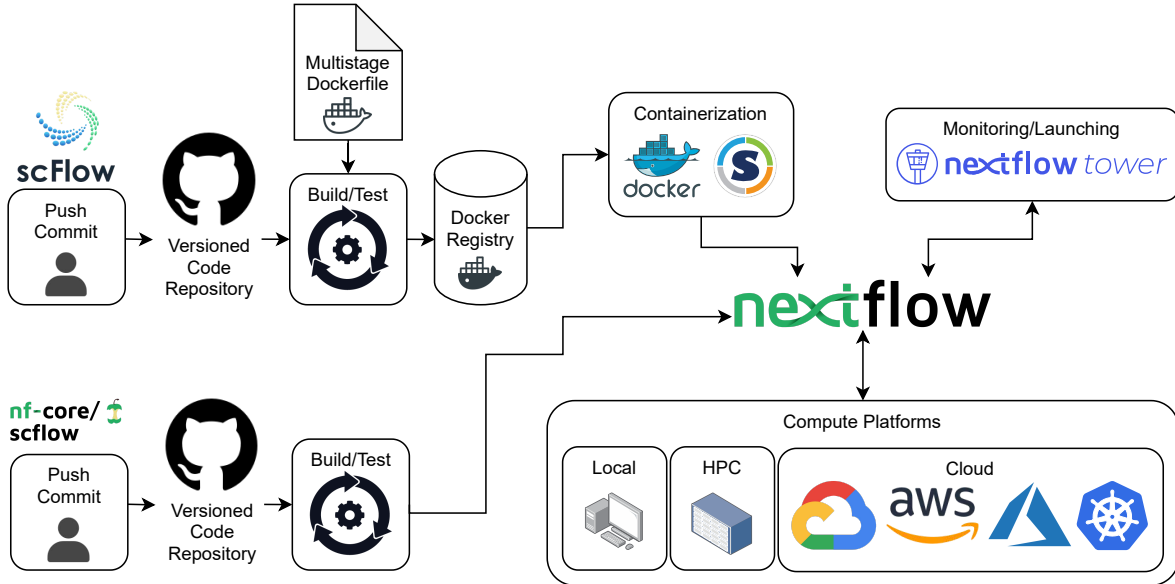


Figure 2: **Workflow for scFlow and nf-core/scflow.** Open-source code for both scFlow and nf-core/scflow is version-controlled and stored in GitHub repositories with continuous integration (CI) to build and test updated code. Container images including software dependencies are automatically built on version updates and uploaded to a Docker registry. Pipeline runs with nf-core/scflow utilize containerized environments using Docker/Singularity to perform analyses reproducibly across diverse compute infrastructure including local workstations, high-performance clusters (HPC), or Cloud services including Google Cloud, Amazon Web Services, Microsoft Azure, and Kubernetes. Real-time monitoring and optional launching of pipeline runs can be performed using NextFlow Tower.

232 **Executing a nf-core/scflow pipeline run**

233 A pipeline run with nf-core/scflow requires three inputs: (1) a two-column manifest file with  
234 paths to gene-cell matrices and a unique sample key; (2) a sample sheet with sample information  
235 for each input matrix in the manifest file; and, (3) a parameters configuration file (documen-  
236 tation for each parameter is available at <https://nf-co.re/scflow/dev/parameters>). A  
237 complete, automated, scalable, and reproducible case-control analysis following the steps in  
238 Figure 1 can then be performed with a single line of code: -

239 `nextflow run nf-core/scflow \`

```
240 --manifest Manifest.tsv \
241 --input Samplesheet.tsv \
242 -c scflow_params.config \
243 -profile local
```

244 Switching from a local workstation analysis to a Cloud based analysis can be achieved simply  
245 by changing the profile parameter. For example, a Google Cloud analysis with automated  
246 staging of input matrices from Cloud storage (e.g. a Google Storage Bucket) can be achieved  
247 using `-profile gcp`. Additionally, pre-configured institutional profiles for a range of university  
248 and research institution HPC systems are readily available via nf-core [<https://github.com/nf-core/configs>].

250 During an nf-core/scflow run, comprehensive pipeline outputs are generated including flat-file  
251 tables, images, and interactive HTML reports. As Nextflow utilizes an intelligent cache based  
252 on hashed inputs to each analytical task, the pipeline can be stopped at any time, parame-  
253 ters adjusted, and the pipeline resumed with the addition of the '`-resume`' option. As only  
254 tasks downstream of the changed parameters are affected and re-run, parameter optimization  
255 is both simplified and accelerated, particularly for the early steps of dimensionality reduction,  
256 clustering, and optional revision of automated cell-type annotations.

257

## 258 METHODS

### 259 Ambient RNA profiling

260 Our implementation of EmptyDrops includes the default options with the emptyDrops R pack-  
261 age, with the following additions. The threshold of UMI counts above which a cellular barcode  
262 will be retained can optionally be determined based on a quantile approach as described previ-  
263 ously and implemented in the CellRanger software by 10X Genomics ([Zheng et al., 2017](#)). This  
264 'auto' option for the retain parameter retains all barcodes with >10% of the counts in the top  
265 nth barcodes, where n is 1% of the expected recovered cell count specified by the 'expect\_-  
266 cells' parameter. The distribution of p-values for presumed ambient barcodes is evaluated for

267 uniformity – as expected under the null-hypothesis – using a Kolmogorov-Smirnov test. De-  
268 fault emptyDrops parameters used by scFlow are: lower=100, retain='auto', expect\_cells=3000,  
269 and niters=30000.

## 270 Thresholding

271 For thresholds determined adaptively, a user-specified number of median absolute deviations  
272 (nMADs) is applied using the Scater package (McCarthy et al., 2017) as previously de-  
273 scribed (Lun et al., 2016b):

274  $MAD(x) = \text{median}(|x_i - \bar{x}|)$ . Default thresholding parameters used by scFlow are: min\_-  
275 library\_size=100, max\_library\_size='adaptive', min\_features=100, max\_features='adaptive',  
276 max\_mito='adaptive', min\_ribo=0, max\_ribo=1, min\_counts=2, min\_cells=2, drop\_un-  
277 mapped=TRUE, drop\_mito=TRUE, drop\_ribo=FALSE, and nmads=4.0. Outliers for inter-  
278 sample post-merge quality-control metrics are determined based on standard deviation ( $\sigma$ )  
279 across samples with warnings provided at the [?]2 $\sigma$  level and alerts at the [?]3 $\sigma$  level.

## 280 Pseudobulking

281 Pseudobulking is performed by summation of counts by sample as previously described (Lun  
282 et al., 2016a). For computational efficiency, the calculations are performed using matrix mul-  
283 tiplication where rows (gene counts) are multiplied by columns of a sample annotation model  
284 matrix:  $c_{ik} = a_{ij}b_{jk}$ .

## 285 Doublet/multiplet detection

286 The DoubletFinder algorithm is implemented essentially as described using the DoubletFinder  
287 R package (McGinnis et al., 2019) with the following additions. A fixed doublet rate, or  
288 alternatively, a doublets-per-thousand-cells increment ('dpk' parameter) can be set to scale the  
289 doublet rate with the number of cells considered, as recommended by 10X Genomics. The 'pK'  
290 parameter can be fixed or determined following a parameter sweep to identify the 'BCmetric'  
291 maxima across a range of 'pK' values, as described in the DoubletFinder vignette. Default  
292 parameters used for DoubletFinder in scFlow are: pca\_dims=20, var\_features=2000, dpk=8,  
293 and pK=0.02.

## 294 Dataset integration

295 LIGER ('rliger' package) was used for dataset integration which uses an integrative non-negative  
296 matrix factorization (iNMF) method to identify shared and dataset-specific factors. The latent  
297 metagene factors are generated as previously described (Welch 2019, Liu 2020). Four pre-  
298 processing steps are applied: (1) normalization for UMIs per cell using 'rliger::normalize', (2)  
299 subsetting the most variable genes for each dataset using 'rliger::selectGenes', (3) scaling by  
300 root-mean-square across cells using 'rliger::scaleNotCenter' to ensure different genes have the  
301 same variance, and (4) filtering of non-expressive genes. For integration, we use the union of  
302 the top 'num\_genes' variable genes from each dataset. To ensure that the union is not signifi-  
303 cantly skewed towards a specific dataset(s), we identify possible outlying dataset(s) using Venn  
304 and UpSet diagrams generated by 'nVennR::plotVenn' (Perez-Silva 2018) and 'UpSetR::upset'  
305 (Conway 2017), respectively. The shared and dataset-specific factors are subsequently gener-  
306 ated from the normalized and scaled inputs using iNMF with the 'rliger::optimizeALS' function.  
307 Finally, the 'rliger::quantile\_norm' function is applied to integrate the datasets together using a  
308 maximum-factor assignment followed by refinement using a k-nearest neighbours (KNN) graph.  
309 Default parameters used for LIGER are: take\_gene\_union=FALSE, remove\_missing=TRUE,  
310 num\_genes=3000, combine="union", capitalize=FALSE, use\_cols=TRUE, k=30, lambda=5.0,  
311 thresh=0.0001, max\_iters=100, nrep=1, rand\_seed=1, knn\_k=20, ref\_dataset=NULL, min\_-  
312 cells=2, quantiles=50, resolution=1 and centre=FALSE. Performance of the integration algo-  
313 rithm is evaluated quantitatively using the kBET algorithm essentially as previously described  
314 (Büttner 2019). A low 'rejection rate' determined by kBET indicates cells from different batches  
315 (and/or other user-defined categorical covariates) are well-mixed.

## 316 Dimensionality reduction

317 The top  $m$  principal components are calculated based on highly variable genes using  
318 'Seurat::RunPCA' for Seurat based sub-workflows, otherwise 'monocle3::preprocess\_cds' is  
319 used. Embeddings for tSNE are generated using 'Seurat::RunTSNE' for Seurat based sub-  
320 workflows, otherwise, Jesse Krijthe's 'Rtsne::Rtsne' implementation of Van der Maaten's Barnes-  
321 Hut algorithm is used [<https://github.com/jkrijthe/Rtsne>]. Default parameters for tS-  
322 NE are: dims=2, initial\_dims=30, perplexity=50, theta=0.5, stop\_lying\_iter=250, mom\_-

323 switch\_iter=250, max\_iter= 1000, pca\_center=TRUE, pca\_scale=FALSE, normalize=TRUE,  
324 momentum=0.5, final\_momentum=0.8, eta=1000, and exaggeration\_factor=12. Embeddings  
325 for UMAP are generated using ‘Seurat::RunUMAP’ for Seurat based sub-workflows, other-  
326 wise, James Melville’s ‘uwot::umap’ implementation of the UMAP algorithm is used [<https://github.com/jlmelville/uwot>]. Default parameters used for UMAP are: pca\_dims=30,  
327 n\_neighbors=35, n\_components=2, init= ‘spectral’, metric=’euclidean’, n\_epochs=200, learn-  
328 ing\_rate=1, min\_dist=0.4, spread=0.85, set\_op\_mix\_ratio=1, local\_connectivity=1, repulsion\_-  
329 strength=1, negative\_sample\_rate=5, and fast\_sgd=FALSE.  
330

### 331 Clustering

332 Clustering of cells using the Louvain or Leiden community detection algorithms is performed  
333 using the ‘monocle3::cluster\_cells’ function, with the modified ability to cluster on any na-  
334 med reducedDims matrix of the SingleCellExperiment object (e.g. UMAP embeddings from  
335 LIGER generated latent factors, UMAP\_Liger). Default parameters are set to cluster\_me-  
336 thod=’leiden’, res=1e-5, k=100, and louvain\_iter=1.

### 337 Cell-type annotation

338 Automated cell-type annotation is performed using the expression weighted cell type enrichment  
339 (EWCE) package essentially as previously described ([Skene and Grant, 2016](#)). Reference data-  
340 sets containing annotated cell-types are first processed using EWCE to produce cell-type data  
341 (‘CTD’) files comprised of cell-type-specific transcriptional signatures. In our analyses, we have  
342 used ‘CTD’ files generated from the Allen human brain atlas ([Hodge et al., 2019](#)) and a mouse  
343 brain dataset ([Zeisel et al., 2015](#)). The top 10% most specific genes are used as marker genes  
344 for each cell-type. Up to  $m$  (default: 10000) cells sampled from the numbered Louvain/Leiden  
345 clusters are evaluated for statistical enrichment in target gene lists of length  $n$  from the re-  
346 ference ‘CTD’ against a background probability distribution generated by 1000 permutations  
347 of random background gene lists of length  $n$ . Each cluster is subsequently annotated with the  
348 highest scoring (lowest adjusted p-value) cell-type and the complete set of results are returned  
349 with the SingleCellExperiment metadata.

## 350 Differential gene expression

351 For DGE, a pre-processing step is first performed to subset genes based on expressivity within a  
352 specific cell-type (default: [?]1 count in [?]10% of cells). Next, the percentage of variance in gene  
353 expression explained by inter-sample variation within a reference class (e.g. healthy/control)  
354 can optionally be calculated using the ‘scater:::getVarianceExplained’ function (McCarthy et al.,  
355 2017). These values are ranked and appended to the output DGE table as an additional  
356 sense check and optional gene list filtering criterion. The proportion of genes detected in each  
357 cell is then calculated and scaled to obtain the cellular detection rate (CDR), as previously  
358 described (Finak et al., 2015):

$$CDR_i = 1/N \sum_{g=1}^N z_{ig}$$

359 Numerical predictors (e.g. age, quantitative histopathology measure) can be scaled and centered  
360 prior to model fitting. Optionally, pseudobulking also can be performed, as described above  
361 (). After pre-processing, DGE models with MAST are performed essentially as previously  
362 described (Finak et al., 2015). A  $\log_2(\text{TPM} + 1)$  expression matrix is calculated from the  
363 raw counts matrix, and a two-part (i.e., including a discrete logistic regression component for  
364 expression rate and a continuous Gaussian component conditioned on each cell expressing a  
365 gene) generalized regression model is fit independently for each gene. The CDR is included as  
366 a covariate alongside additional user-specified experimental covariates, which can include, for  
367 example, the individual sample as a random effect (Zimmerman et al., 2021). False-discovery  
368 rate (FDR) adjusted p-values are determined using the Benjamini & Hochberg method.

## 369 Impacted pathway analysis

370 Enrichment of gene lists in pathways are evaluated using methods encompassing Over Repre-  
371 sentation Analysis (ORA) (Khatri et al., 2012), Gene Set Enrichment Analysis (GSEA) (Sub-  
372 ramanian et al., 2005), and Network Topology-based Analysis (Wang et al., 2017). Databases  
373 and methods from one or more of the R packages WebGestaltR (Liao et al., 2019), ROnto-  
374 Tools (Mitrea et al., 2013), and enrichR (Chen et al., 2013) are applied as previously described,

375 and can be queried simultaneously. Results are returned as standard tool output tables and dot  
376 plots of enrichment/odds ratio vs adjusted p-values (FDR) for the top  $n$  pathways are generated  
377 and collated into an IPA HTML report.

### 378 **Dirichlet modeling of cell-type composition**

379 To identify statistical differences in cell-type proportions between categorical dependent vari-  
380 ables (e.g. case vs control), a Dirichlet multinomial regression is performed (Smillie et al.,  
381 2019). A sample (rows) by cell-types (columns) matrix of cell numbers is generated and nor-  
382 malized to relative proportions (0, 1) such that the sum of proportions of each cell-type  $c$  in  
383 sample  $y$  equals one:  $\sum_{c=1}^C y_c = 1$ . If extreme values of 0 or 1 are present, a transforma-  
384 tion is applied using the DirichletReg R package to shrink values away from these extremes  
385 by transforming each component  $y$  of  $Y$  by computing  $y* = [y(n - 1) + 1/d]/n$  where  $n$  is  
386 the number of observations in  $Y$ , as implemented in the ‘DR\_data’ function in the R package  
387 DirichletReg (Maier, 2014). The “common” model (counts ~ dependent\_variable) is fit using  
388 the ‘DirichletReg::DirichReg’ function and p-values are extracted. Bar plots for each cell-type  
389 are generated and collated with input and output tables for the cell-type proportions HTML  
390 report.

### 391 **Dataset pre-processing**

392 Inputs for scFlow are standardized sparse-matrices generated by widely-used pipelines (e.g.  
393 Cell Ranger) for processing, reference genome mapping, and de-multiplexing of raw single-cell  
394 sequencing data (Zheng et al., 2017). As public datasets vary with respect to data deposition  
395 format, custom scripts were required for each of the four analysed datasets to (a) pre-process  
396 matrices into standard per-sample gene-cell counts matrices and/or (b) build a sample sheet with  
397 pertinent experimental data attached. Raw gene-cell count matrix and sample-level metadata  
398 for (Mathys et al., 2019) and the human dataset for (Zhou et al., 2020) were downloaded from the  
399 AD Knowledge Portal [<https://www.synapse.org>] (Synapse ID: syn18485175) and the count  
400 matrix for the respective dataset was split into per sample gene-cell count matrices. Mouse  
401 datasets (Zhou et al., 2020)(Ximerakis et al., 2019) were downloaded from GEO (<https://www.ncbi.nlm.nih.gov/geo/>) (ID:GSE140511 and GSE129788, respectively) and split into per

403 sample gene-cell count matrices. The feature names for gene-cell count matrices from (Ximerakis  
404 et al., 2019) were mouse gene symbols which were first converted to mouse Ensembl IDs. All data  
405 preprocessing scripts are available at [https://github.com/combiz/scFlow\\_Supplementary](https://github.com/combiz/scFlow_Supplementary).

## 406 Nextflow

407 The nf-core/scflow pipeline was coded in Nextflow with domain-specific language 2 (DSL2) ac-  
408 cording to nf-core guidelines. The major analytical steps outlined in Figure 1 are performed  
409 across Nextflow processes implemented in DSL2 modules as detailed in (S??). Included are de-  
410 tails of the underlying scFlow functions utilized for each process, an overview of process outputs,  
411 and parallelization support (i.e. simultaneous analysis of multiple samples/models across multi-  
412 ple independent compute instances/jobs). These processes represent modular units of pipeline  
413 execution in Nextflow, simplifying the modification of individual pipeline steps, and allowing  
414 process-level resource allocation. Detailed information on pipeline usage, parameters, and  
415 outputs are provided in the nf-core/scflow documentation online [<https://nf-co.re/scflow>].

## 416 Software availability

417 The code for the scFlow R package is available in a GitHub repository  
418 [<https://github.com/combiz/scflow>] with associated function documentation  
419 at <https://combiz.github.io/scFlow>. The code for the nf-core/scflow pipeline is avail-  
420 able in a GitHub repository [<https://github.com/nf-core/scflow>] with pipeline  
421 documentation at <https://nf-co.re/scflow>. A general usage manual is available  
422 at <https://combiz.github.io/scflow-manual/>. All code is open-source and available under  
423 the GNU General Public License v3.0 (GPL-3).

424

## 425 Results

426 To demonstrate the performance and flexibility of scFlow for automated case-control sc/sn-  
427 RNA seq analyses, four previously published datasets were retrieved from online repositories,  
428 pre-processed, and submitted to nf-core/scflow for analysis with a single line of code (Mathys

429 et al., 2019; Ximerakis et al., 2019; Zhou et al., 2020). These studies encompass samples from  
430 both human and mouse species, include both single-cell and single-nuclei data, span a range of  
431 samples per study (12 - 48), and each represent a different type of experimental design with  
432 different confounds and variables of interest (Table 1).

Dataset	Species	Input	Sam-	Disease	Tis-	Cell/Nuclei	Plat-
		matrices	ples		sue		form
Mathys <i>et al.</i> , 2019	Hu- man	Raw	48	Alzheimer's	Brain	Nuclei	10X
Zhou <i>et al.</i> , 2020	Hu- man	Filtered	22	Alzheimer's	Brain	Nuclei	10X
Zhou <i>et al.</i> , 2020	Mouse	Filtered	12	Alzheimer's (model)	Brain	Nuclei	10X
Ximerakis <i>et al.</i> , 2019	Mouse	Filtered	16	Aging	Brain	Cell	10X

Table 1: Characteristics of individual datasets analysed in this study with nf-core/scflow.

433 Selected cell-level quality-control metrics and cell/gene-level inclusion and exclusion QC checks  
434 presented here highlight the valuable quality-control data captured by the pipeline (Figure 3). The complete set of pipeline QC outputs are included in the supplemental materials  
435 (e.g. per-sample QC reports, study post-merge reports, QC metrics summary table). The  
436 extensive variation between samples within - and across - studies that is apparent illustrates  
437 the importance of tailored thresholding (e.g. minimum and maximum counts, features, relative  
438 mitochondrial counts, etc.) and the potential benefits of identifying sample-level outliers.

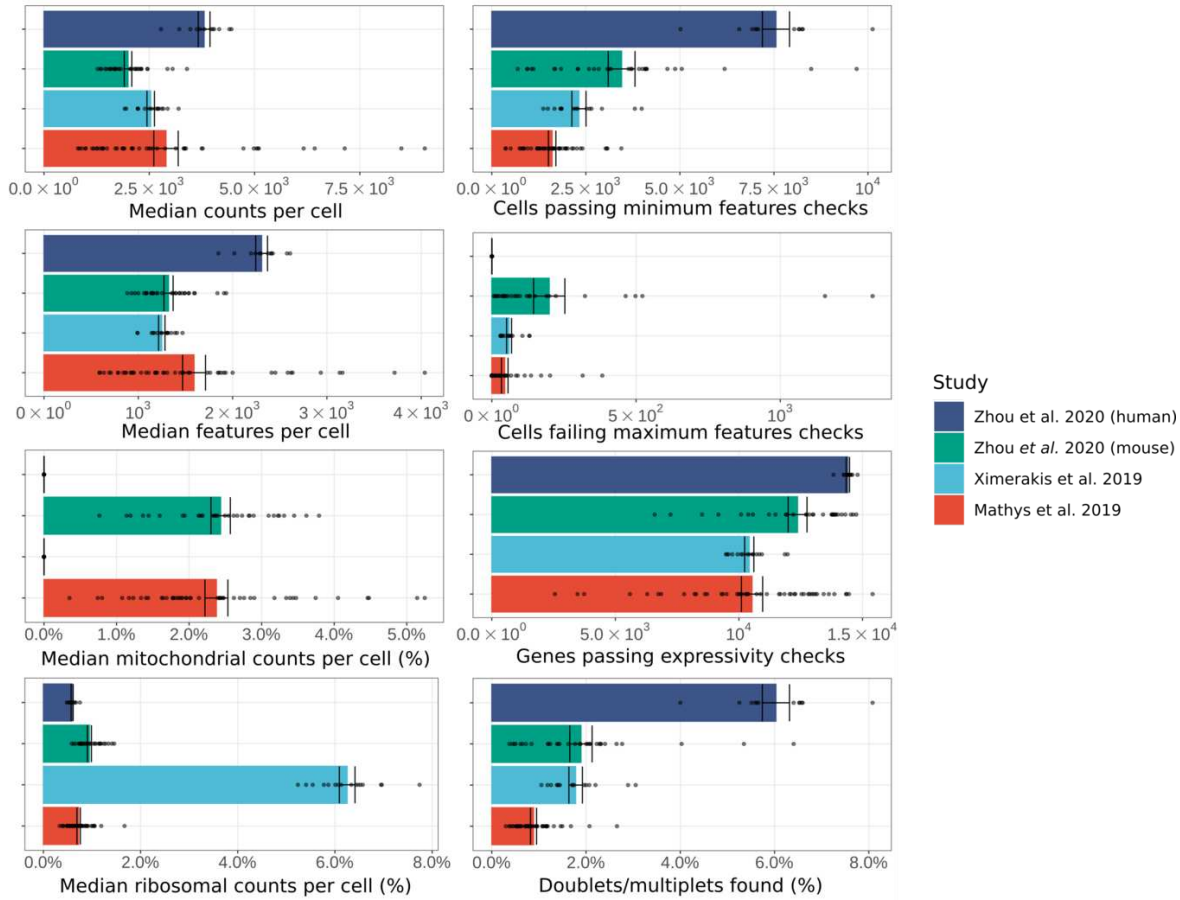


**Figure 3: Selected quality-control metrics in 98 samples across four datasets.** The mean ( $\bar{x} \pm \text{SEM}$ ) of the sample-level medians (points) of four key cell-level metrics – total counts, total genes, relative mitochondrial counts, and relative ribosomal counts – are presented for each of the four analysed datasets (colours) in the left column. The right column includes examples of cell- and gene-level quality control inclusion and exclusion checks used for filtering of input matrices for downstream analyses.

440 The UMAP embeddings with cell-type annotations show a good separation (global distance)  
 441 between major cell-types (e.g. oligodendrocytes and astrocytes) with relative proximity of rela-  
 442 ted cell-types (e.g. neuronal sub-types) for each of the four datasets, as expected (Figure 4a).  
 443 Additionally, the cell-type markers identified by the pipeline are consistent with known markers  
 444 for the cell-types (see supplemental data, cell-type metrics reports). The UMAP embeddings  
 445 for all four datasets were generated from latent metagene factors computed by LIGER. This  
 446 integration approach leads to UMAP embeddings that are less driven by known sources of va-

447 variation in the data (e.g. diagnosis, age, genotype). This is demonstrated both visually – by  
448 contrast to a unintegrated (left) UMAP (Figure 4b) – and by a reduced kBET ‘rejection rate’,  
449 reflecting improved cell mixing (Figure 4c). Improved integration across multiple additional  
450 sources of sample-level variance (e.g. individual, sex) are also evident (see supplemental data,  
451 integration reports). Together these provide evidence that integration of the data was effective,  
452 with a greater contribution of shared, relative to sample-specific, factors to the separation of  
453 cells in reduced dimensional space.

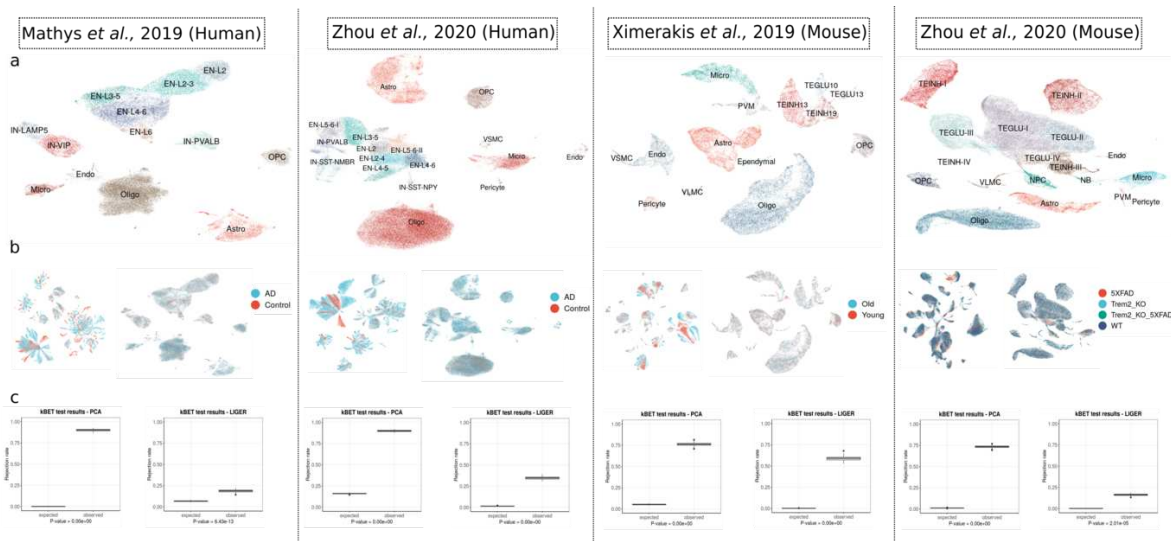
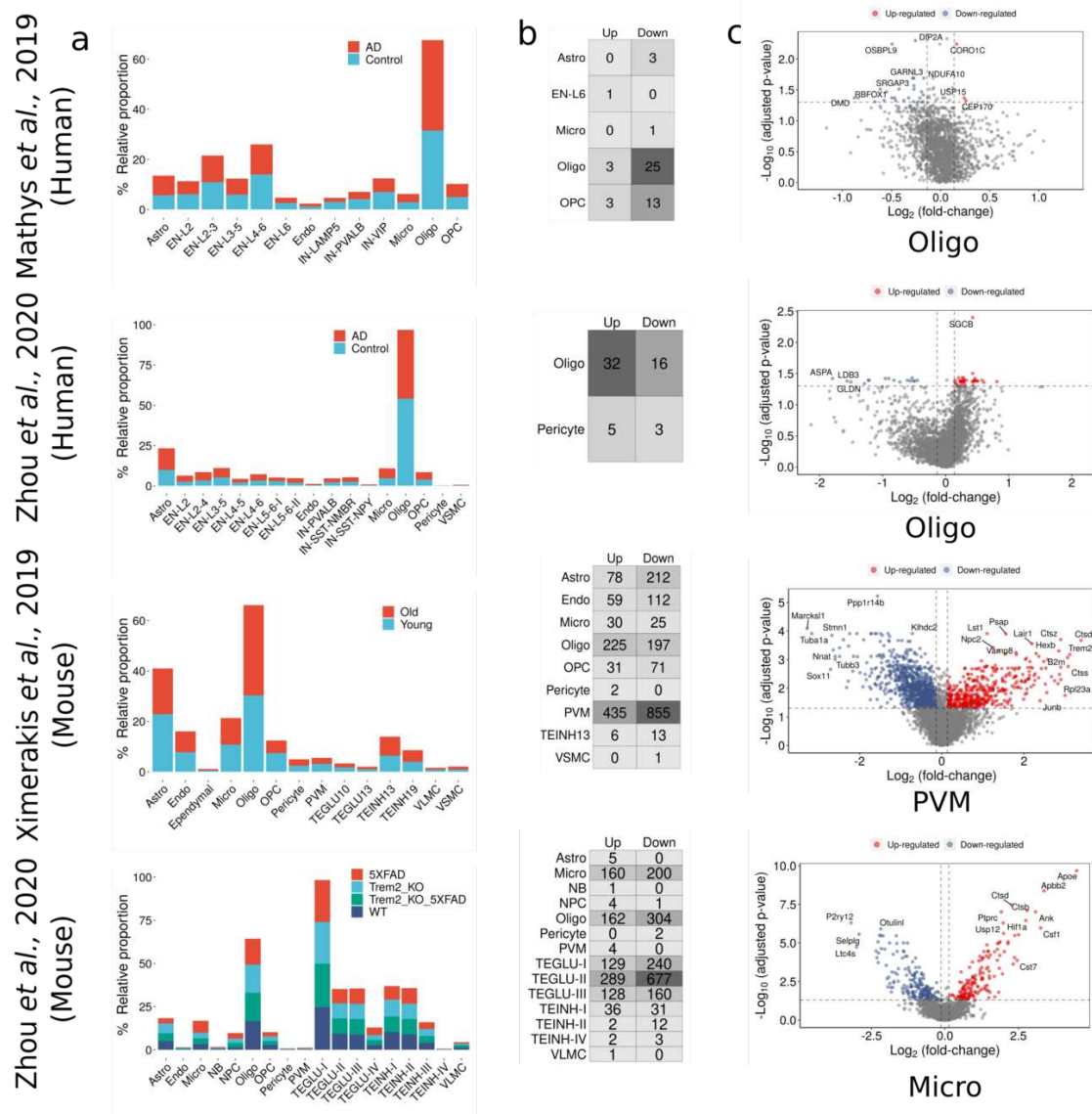


Figure 4: **Cell-type annotation and key integration results from the analysis of four datasets with the nf-core/scflow pipeline.** For each study, a) UMAP plot of the final clusters with their cell-type annotations, b) UMAP of an unintegrated (left) and LIGER-integrated (right) dataset highlighting the categorical variable of interest, c) box plots of expected and observed kBET ‘rejection rates’ from unintegrated (left) and LIGER-integrated (right) UMAPs.

454 The relative proportion of cell-types in each study, further stratified by the major dependent  
455 variable of interest, is summarized in Figure 5a. Differential gene expression was evaluated  
456 in each cell-type using a mixed-model in MAST with a random effect for individual. The  
457 number of differentially expressed genes identified as up-regulated and down-regulated for each  
458 cell-type are highlighted (Figure 4b). For a selected cell-type from each study, the number,  
459 significance (adjusted p-value), and magnitude (fold-change) of evaluated genes are illustrated

460 in a volcano plot (Figure 4c). Although an in-depth contrast of our results with those in  
461 the original studies is beyond the scope of this manuscript, the identification of the canonical  
462 Alzheimer's disease implicated gene 'Apoe' in the microglia of mouse cells in the Alzheimer's  
463 mouse dataset from Zhou *et al.* provides an example of the potential for insight discovery  
464 using our pipeline. Overall, these results, associated with similarly identified cells and derived  
465 using the same, well-controlled analytical pipeline and parameters, highlight the clear differences  
466 between differentially expressed gene sets from different studies and tissue types. By doing so,  
467 they also allow more confident generalisations regarding those features that are reproducible  
468 (e.g., the greater complexity and numbers of significantly differentially expressed genes in the  
469 rapidly isolated single-cell mouse brain transcriptomes relative to those in the human single  
470 nuclear transcriptomes from post mortem brain tissue).



**Figure 5: Relative cell-type proportions and summary of differential expression analysis results.** a) Bar plots showing the relative proportions of cell-types between the categorical variables of interest for each of the datasets, b) Numbers of statistically significant up and down-regulated genes per cell-type; cell-types for which no differential expressed genes were found were omitted, c) Volcano plots of differentially expressed genes for the specified cell types of the four datasets.

## 471 Discussion

472 The use of pipelines for the analysis of large datasets involving multiple, complex analytical steps  
473 is essential to achieve reproducible results. The wide range of alternative tools available for most  
474 analytical steps of single-cell RNA sequencing, combined with the different experimental ques-  
475 tions and confounds particular to each dataset, often leads to project-specific code. These would  
476 typically require the manual revision of code to analyze a new dataset or to utilize an alternative  
477 algorithm for an analytical step. The scFlow toolkit and nf-core/scflow pipeline address this  
478 by implementing standardized, modular code: the flexibility to handle complex experimental  
479 designs and apply alternative algorithms are handled at the level of parameter specification.  
480 This modular approach also lends itself well to extensibility, as new tools in the field may be  
481 readily incorporated for an individual analytical task. The decoupling of analysis logic from  
482 resource allocation by Nextflow provides portability and scalability, with nf-core/scflow ready  
483 to run on local workstations, HPC environments, and Cloud services including Google Cloud,  
484 Amazon Web Services, and Microsoft Azure. This scalability will allow scFlow to keep pace  
485 with the burgeoning scale of single-cell RNA sequencing datasets.

486 The use of containerization technology by nf-core/scflow provides a consistent computing en-  
487 vironment to ensure that the complex software and system dependencies used for analysis are  
488 comprehensively captured and are re-usable. Taken together with the version-control of pipeline  
489 code, and the generation of a citable unique digital object identifier (DOI) via nf-core for each  
490 versioned update to the pipeline, there is reassurance both of the reproducibility and the citabil-  
491 ity of an analysis.

492 We expect that the ease-of-use of nf-core/scflow and its flexibility to integrate datasets should  
493 be particularly useful for case-control and joint studies, including cell-atlas projects where data  
494 may be generated at different sites using different scRNA-seq protocols. The ability to adap-  
495 tively threshold samples and evaluate inter-sample quality-control metrics can inform sample  
496 inclusion/exclusion criteria and potentially greatly improve the quality of such data resources.

497 In summary, the scFlow toolkit and nf-core/scflow pipeline provide a robust and easy-to-use  
498 analysis approach, leveraging the best scRNA-seq analysis tools in the R ecosystem with state-  
499 of-the-art data science to provide scalable, reproducible, and extensible analyses of scRNA-seq

500 data.

## 501 Acknowledgements

502 CK is grateful to the Imperial College London NIHR Biomedical Research Centre Brain Sciences  
503 Theme for funding for his work. NS acknowledges support from UKRI Future Leaders Fellow-  
504 ship [grant number MR/T04327X/1]. PMM acknowledges generous personal support from the  
505 Edmond J Safra Foundation and Lily Safra and an NIHR Senior Investigator Award. This work  
506 was supported by the UK Dementia Research Institute, which receives its funding from UK DRI  
507 Ltd., funded by the UK Medical Research Council, Alzheimer's Society and Alzheimer's Re-  
508 search UK, and the Imperial College London NIHR Biomedical Research Centre.

509 We are grateful for helpful comments from members of the Nextflow and nf-core teams, in  
510 particular Paolo Di Tommaso, Philip A. Ewels, Harshil Patel, Alexander Peltzer, and Maxime  
511 Ulysse Garcia, and lab members including Johanna Jackson, Amy Smith, Karen Davey, and  
512 Stergios Tsartsalis.

## 513 Declarations

514 PMM has received consultancy fees from Roche, Adelphi Communications, Celgene, Neurodiem  
515 and Medscape. He has received honoraria or speakers' fees from Novartis and Biogen and has  
516 received research or educational funds from Biogen, Novartis and GlaxoSmithKline.

## 517 Supplementary Material

### 518 Hosted file

519 [Supplementary\\_Table\\_2\\_Process\\_Summary.xlsx](https://authorea.com/users/226952/articles/480342-scflow-a-scalable-and-reproducible-analysis-pipeline-for-single-cell-rna-sequencing-data) available at <https://authorea.com/users/226952/articles/480342-scflow-a-scalable-and-reproducible-analysis-pipeline-for-single-cell-rna-sequencing-data>

522 **Hosted file**

523 `Supplemental_software_versions.tsv` available at <https://authorea.com/users/226952/articles/480342-scflow-a-scalable-and-reproducible-analysis-pipeline-for-single-cell-rna-sequencing-data>

526 **Hosted file**

527 `Supplemental_Reports_Info.md` available at <https://authorea.com/users/226952/articles/480342-scflow-a-scalable-and-reproducible-analysis-pipeline-for-single-cell-rna-sequencing-data>

530 **References**

531 S Aldridge and SA Teichmann. Single cell transcriptomics comes of age. *Nat Commun*, 11: 4307, Aug 2020.

533 RA Amezquita, ATL Lun, E Becht, VJ Carey, LN Carpp, L Geistlinger, F Marini, K Rue-Albrecht, D Risso, C Soneson, L Waldron, H Pagès, ML Smith, W Huber, M Morgan, R Got-tardo, and SC Hicks. Orchestrating single-cell analysis with Bioconductor. *Nat Methods*, 17: 137–145, Feb 2020.

537 M Baker. 1,500 scientists lift the lid on reproducibility. *Nature*, 533:452–4, May 2016.

538 E Becht, L McInnes, J Healy, CA Dutertre, IWH Kwok, LG Ng, F Ginhoux, and EW Newell. Dimensionality reduction for visualizing single-cell data using UMAP. *Nat Biotechnol*, Dec 2018.

541 J Cao, M Spielmann, X Qiu, X Huang, DM Ibrahim, AJ Hill, F Zhang, S Mundlos, L Chris-tiansen, FJ Steemers, C Trapnell, and J Shendure. The single-cell transcriptional landscape of mammalian organogenesis. *Nature*, 566:496–502, Feb 2019.

544 EY Chen, CM Tan, Y Kou, Q Duan, Z Wang, GV Meirelles, NR Clark, and A Ma'ayan. Enrichr: interactive and collaborative HTML5 gene list enrichment analysis tool. *BMC Bioinformatics*, 14:128, Apr 2013.

547 Tommaso P Di, M Chatzou, EW Floden, PP Barja, E Palumbo, and C Notredame. Nextflow  
548 enables reproducible computational workflows. *Nat Biotechnol*, 35:316–319, Apr 2017.

549 M Eisenstein. Single-cell RNA-seq analysis software providers scramble to offer solutions. *Nat*  
550 *Biotechnol*, 38:254–257, Mar 2020.

551 PA Ewels, A Peltzer, S Fillinger, H Patel, J Alneberg, A Wilm, MU Garcia, Tommaso P Di,  
552 and S Nahnse. The nf-core framework for community-curated bioinformatics pipelines. *Nat*  
553 *Biotechnol*, 38:276–278, Mar 2020.

554 G Finak, A McDavid, M Yajima, J Deng, V Gersuk, AK Shalek, CK Slichter, HW Miller,  
555 MJ McElrath, M Prlic, PS Linsley, and R Gottardo. MAST: a flexible statistical framework  
556 for assessing transcriptional changes and characterizing heterogeneity in single-cell RNA se-  
557 quencing data. *Genome Biol*, 16:278, Dec 2015.

558 B Gruening, O Sallou, P Moreno, Veiga Leprevost F da, H Ménager, D Søndergaard, H Röst,  
559 T Sachsenberg, B O'Connor, F Madeira, Del Angel V Dominguez, MR Crusoe, S Varma,  
560 D Blankenberg, RC Jimenez, and Y Perez-Riverol. Recommendations for the packaging and  
561 containerizing of bioinformatics software. *F1000Res*, 7, 2018.

562 Björn Grüning, John Chilton, Johannes Köster, Ryan Dale, Nicola Soranzo, Marius van den  
563 Beek, Jeremy Goecks, Rolf Backofen, Anton Nekrutenko, and James Taylor. Practical Com-  
564 putational Reproducibility in the Life Sciences. *Cell Systems*, 6(6):631–635, jun 2018. doi:  
565 10.1016/j.cels.2018.03.014. URL <https://doi.org/10.1016%2Fj.cels.2018.03.014>.

566 Y Hao, S Hao, E Andersen-Nissen, WM 3rd Mauck, S Zheng, A Butler, MJ Lee, AJ Wilk,  
567 C Darby, M Zager, P Hoffman, M Stoeckius, E Papalexi, EP Mimitou, J Jain, A Srivastava,  
568 T Stuart, LM Fleming, B Yeung, AJ Rogers, JM McElrath, CA Blish, R Gottardo, P Smibert,  
569 and R Satija. Integrated analysis of multimodal single-cell data. *Cell*, 184:3573–3587.e29,  
570 Jun 2021.

571 CN Heiser and KS Lau. A Quantitative Framework for Evaluating Single-Cell Data Structure  
572 Preservation by Dimensionality Reduction Techniques. *Cell Rep*, 31:107576, May 2020.

573 RD Hodge, TE Bakken, JA Miller, KA Smith, ER Barkan, LT Graybuck, JL Close, B Long,  
574 N Johansen, O Penn, Z Yao, J Eggemont, T Höllt, BP Levi, SI Shehata, B Aevermann,

575 A Beller, D Bertagnolli, K Brouner, T Casper, C Cobbs, R Dalley, N Dee, SL Ding, RG El-  
576 lenbogen, O Fong, E Garren, J Goldy, RP Gwinn, D Hirschstein, CD Keene, M Keshk, AL Ko,  
577 K Lathia, A Mahfouz, Z Maltzer, M McGraw, TN Nguyen, J Nyhus, JG Ojemann, A Oldre,  
578 S Parry, S Reynolds, C Rimorin, NV Shapovalova, S Somasundaram, A Szafer, ER Thom-  
579 sen, M Tieu, G Quon, RH Scheuermann, R Yuste, SM Sunkin, B Lelieveldt, D Feng, L Ng,  
580 A Bernard, M Hawrylycz, JW Phillips, B Tasic, H Zeng, AR Jones, C Koch, and ES Lein.  
581 Conserved cell types with divergent features in human versus mouse cortex. *Nature*, 573:  
582 61–68, Sep 2019.

583 P Khatri, C Voichita, K Kattan, N Ansari, A Khatri, C Georgescu, AL Tarca, and S Draghici.  
584 Onto-Tools: new additions and improvements in 2006. *Nucleic Acids Res*, 35:W206–11, Jul  
585 2007.

586 P Khatri, M Sirota, and AJ Butte. Ten years of pathway analysis: current approaches and  
587 outstanding challenges. *PLoS Comput Biol*, 8:e1002375, 2012.

588 D Kobak and P Berens. The art of using t-SNE for single-cell transcriptomics. *Nat Commun*,  
589 10:5416, Nov 2019.

590 MV Kuleshov, MR Jones, AD Rouillard, NF Fernandez, Q Duan, Z Wang, S Koplev, SL Jenkins,  
591 KM Jagodnik, A Lachmann, MG McDermott, CD Monteiro, GW Gundersen, and A Ma'ayan.  
592 Enrichr: a comprehensive gene set enrichment analysis web server 2016 update. *Nucleic Acids  
Res*, 44:W90–7, Jul 2016.

594 Y Liao, J Wang, EJ Jaehnig, Z Shi, and B Zhang. WebGestalt 2019: gene set analysis toolkit  
595 with revamped UIs and APIs. *Nucleic Acids Res*, 47:W199–W205, Jul 2019.

596 MD Luecken and FJ Theis. Current best practices in single-cell RNA-seq analysis: a tutorial.  
597 *Mol Syst Biol*, 15:e8746, Jun 2019.

598 AT Lun, K Bach, and JC Marioni. Pooling across cells to normalize single-cell RNA sequencing  
599 data with many zero counts. *Genome Biol*, 17:75, Apr 2016a.

600 AT Lun, DJ McCarthy, and JC Marioni. A step-by-step workflow for low-level analysis of  
601 single-cell RNA-seq data with Bioconductor. *F1000Res*, 5:2122, 2016b.

602 ATL Lun, S Riesenfeld, T Andrews, TP Dao, T Gomes, and JC Marioni. EmptyDrops: distin-

603 guishing cells from empty droplets in droplet-based single-cell RNA sequencing data. *Genome*  
604 *Biol*, 20:63, Mar 2019.

605 Marco J. Maier. DirichletReg: Dirichlet Regression for Compositional Data in R - ePubWU.  
606 Technical report, 2014. URL <https://epub.wu.ac.at/4077/>. Accessed on Tue, August 10,  
607 2021.

608 H Mathys, J Davila-Velderrain, Z Peng, F Gao, S Mohammadi, JZ Young, M Menon, L He,  
609 F Abdurrob, X Jiang, AJ Martorell, RM Ransohoff, BP Hafler, DA Bennett, M Kellis, and  
610 LH Tsai. Single-cell transcriptomic analysis of Alzheimer's disease. *Nature*, 570:332–337, Jun  
611 2019.

612 DJ McCarthy, KR Campbell, AT Lun, and QF Wills. Scater: pre-processing, quality control,  
613 normalization and visualization of single-cell RNA-seq data in R. *Bioinformatics*, 33:1179–  
614 1186, Apr 2017.

615 CS McGinnis, LM Murrow, and ZJ Gartner. DoubletFinder: Doublet Detection in Single-Cell  
616 RNA Sequencing Data Using Artificial Nearest Neighbors. *Cell Syst*, 8:329–337.e4, Apr 2019.

617 V Menon. Clustering single cells: a review of approaches on high-and low-depth single-cell  
618 RNA-seq data. *Brief Funct Genomics*, 18:434, Nov 2019.

619 C Mitrea, Z Taghavi, B Bokanizad, S Hanoudi, R Tagett, M Donato, C Voichița, and S Drăghici.  
620 Methods and approaches in the topology-based analysis of biological pathways. *Front Physiol*,  
621 4:278, Oct 2013.

622 JM Perkel. Challenge to scientists: does your ten-year-old code still run? *Nature*, 584:656–658,  
623 Aug 2020.

624 F Raimundo, C Vallot, and JP Vert. Tuning parameters of dimensionality reduction methods  
625 for single-cell RNA-seq analysis. *Genome Biol*, 21:212, Aug 2020.

626 SA Sansone, P McQuilton, P Rocca-Serra, A Gonzalez-Beltran, M Izzo, AL Lister, and  
627 M Thurston. FAIRsharing as a community approach to standards, repositories and poli-  
628 cies. *Nat Biotechnol*, 37:358–367, Apr 2019.

629 E Shema, BE Bernstein, and JD Buenrostro. Single-cell and single-molecule epigenomics to  
630 uncover genome regulation at unprecedented resolution. *Nat Genet*, 51:19–25, Jan 2019.

631 NG Skene and SG Grant. Identification of Vulnerable Cell Types in Major Brain Disorders  
632 Using Single Cell Transcriptomes and Expression Weighted Cell Type Enrichment. *Front*  
633 *Neurosci*, 10:16, 2016.

634 CS Smillie, M Biton, J Ordovas-Montanes, KM Sullivan, G Burgin, DB Graham, RH Herbst,  
635 N Rogel, M Slyper, J Waldman, M Sud, E Andrews, G Velonias, AL Haber, K Jagadeesh,  
636 S Vickovic, J Yao, C Stevens, D Dionne, LT Nguyen, AC Villani, M Hofree, EA Creasey,  
637 H Huang, O Rozenblatt-Rosen, JJ Garber, H Khalili, AN Desch, MJ Daly, AN Ananthakr-  
638 ishnan, AK Shalek, RJ Xavier, and A Regev. Intra- and Inter-cellular Rewiring of the Human  
639 Colon during Ulcerative Colitis. *Cell*, 178:714–730.e22, Jul 2019.

640 A Subramanian, P Tamayo, VK Mootha, S Mukherjee, BL Ebert, MA Gillette, A Paulovich,  
641 SL Pomeroy, TR Golub, ES Lander, and JP Mesirov. Gene set enrichment analysis: a  
642 knowledge-based approach for interpreting genome-wide expression profiles. *Proc Natl Acad*  
643 *Sci U S A*, 102:15545–50, Oct 2005.

644 M Tekman, B Batut, A Ostrovsky, C Antoniewski, D Clements, F Ramirez, GJ Etherington,  
645 HR Hotz, J Scholtalbers, JR Manning, L Bellenger, MA Doyle, M Heydarian, N Huang,  
646 N Soranzo, P Moreno, S Mautner, I Papatheodorou, A Nekrutenko, J Taylor, D Blankenberg,  
647 R Backofen, and B Grüning. A single-cell RNA-sequencing training and analysis suite using  
648 the Galaxy framework. *Gigascience*, 9, Oct 2020.

649 VA Traag, L Waltman, and Eck NJ van. From Louvain to Leiden: guaranteeing well-connected  
650 communities. *Sci Rep*, 9:5233, Mar 2019.

651 C Trapnell, D Cacchiarelli, J Grimsby, P Pokharel, S Li, M Morse, NJ Lennon, KJ Livak,  
652 TS Mikkelsen, and JL Rinn. The dynamics and regulators of cell fate decisions are revealed  
653 by pseudotemporal ordering of single cells. *Nat Biotechnol*, 32:381–386, Apr 2014.

654 J Wang, Z Ma, SA Carr, P Mertins, H Zhang, Z Zhang, DW Chan, MJ Ellis, RR Townsend,  
655 RD Smith, JE McDermott, X Chen, AG Paulovich, ES Boja, M Mesri, CR Kinsinger, H Ro-  
656 driguez, KD Rodland, DC Liebler, and B Zhang. Proteome Profiling Outperforms Transcrip-

657 tome Profiling for Coexpression Based Gene Function Prediction. *Mol Cell Proteomics*, 16:  
658 121–134, Jan 2017.

659 JD Welch, V Kozareva, A Ferreira, C Vanderburg, C Martin, and EZ Macosko. Single-Cell  
660 Multi-omic Integration Compares and Contrasts Features of Brain Cell Identity. *Cell*, 177:  
661 1873–1887.e17, Jun 2019.

662 M Ximerakis, SL Lipnick, BT Innes, SK Simmons, X Adiconis, D Dionne, BA Mayweather,  
663 L Nguyen, Z Niziolek, C Ozek, VL Butty, R Isserlin, SM Buchanan, SS Levine, A Regev,  
664 GD Bader, JZ Levin, and LL Rubin. Single-cell transcriptomic profiling of the aging mouse  
665 brain. *Nat Neurosci*, 22:1696–1708, Oct 2019.

666 A Zeisel, AB Muñoz-Manchado, S Codeluppi, P Lönnerberg, Manno G La, A Juréus, S Mar-  
667 ques, H Munguba, L He, C Betsholtz, C Rolny, G Castelo-Branco, J Hjerling-Leffler, and  
668 S Linnarsson. Brain structure. Cell types in the mouse cortex and hippocampus revealed by  
669 single-cell RNA-seq. *Science*, 347:1138–42, Mar 2015.

670 GX Zheng, JM Terry, P Belgrader, P Ryvkin, ZW Bent, R Wilson, SB Ziraldo, TD Wheeler,  
671 GP McDermott, J Zhu, MT Gregory, J Shuga, L Montesclaros, JG Underwood, DA Masque-  
672 lier, SY Nishimura, M Schnall-Levin, PW Wyatt, CM Hindson, R Bharadwaj, A Wong,  
673 KD Ness, LW Beppu, HJ Deeg, C McFarland, KR Loeb, WJ Valente, NG Ericson,  
674 EA Stevens, JP Radich, TS Mikkelsen, BJ Hindson, and JH Bielas. Massively parallel digital  
675 transcriptional profiling of single cells. *Nat Commun*, 8:14049, Jan 2017.

676 Y Zhou, WM Song, PS Andhey, A Swain, T Levy, KR Miller, PL Poliani, M Cominelli, S Grover,  
677 S Gilfillan, M Cellai, TK Ulland, K Zaitsev, A Miyashita, T Ikeuchi, M Sainouchi, A Kakita,  
678 DA Bennett, JA Schneider, MR Nichols, SA Beausoleil, JD Ulrich, DM Holtzman, MN Arty-  
679 omov, and M Colonna. Human and mouse single-nucleus transcriptomics reveal TREM2-  
680 dependent and TREM2-independent cellular responses in Alzheimer's disease. *Nat Med*, 26:  
681 131–142, Jan 2020.

682 KD Zimmerman, MA Espeland, and CD Langefeld. A practical solution to pseudoreplication  
683 bias in single-cell studies. *Nat Commun*, 12:738, Feb 2021.